

DETC2007-35368

SOFTWARE FOR INVESTIGATING THE KINEMATICS, STATICS AND DYNAMICS OF COUPLER-DRIVEN FOUR-BARS FOR TWO POSITION SYNTHESIS

Michael L. Turner,* Eric M. Grimm, Daniel Debrosse, Kevin Kosmac and Andrew P. Murray
Department of Mechanical and Aerospace Engineering
University of Dayton
Dayton, OH 45469-0238
Email: michael.turner@notes.udayton.edu

ABSTRACT

The synthesis of a planar four-bar in which a point on the coupler reaches two specified points and orientations generates a six-fold space of solutions. The solution space increases if additional links are added to drive the mechanism, such as the Stephenson III. This paper presents an investigation of a coupler driven four-bar linkage, a Stephenson III six-bar with an RPR chain driving the four-bar sub-chain instead of the classically defined 3R chain. The software allows the designer to specify the problem and quickly scan the solution space. A comparison is constructed between a four-bar driven through a torque at the input link and a coupler-driven four-bar. Changes in branch points, the joint force index and the dynamics are observed.

NOMENCLATURE

General Vector Notation

\vec{V} The [x,y] vector V, may be associated with an object V such as a joint or link

v The length of \vec{V}

θ_V The angular orientation of \vec{V} with respect to the planar x-axis according to the right hand rule.

ω_V Angular velocity, the time derivative of θ_V

α_V Angular acceleration, the time derivative of ω_V

m_V The mass of link V

I_V The moment of inertia of link V

Some specific vectors

- \vec{G}_n The location of the fixed pivot G_n in the plane
- \vec{Z}_n The location of the moving pivot Z_n in the plane
- \vec{E}_n Coupler point, the location in the plane of the n-th position a point of the coupler must reach
- ϕ_n The target orientation of the coupler point in the n-th position
- \vec{I} The location in the plane of the instant center of the coupler with respect to ground.

INTRODUCTION

The synthesis of a four-bar mechanism to move an object from one position to another position is a well studied problem. [1] [2] [3] If the object is attached to the coupler of the four-bar, the designer is faced with a large number of valid solutions, and it may be difficult to assess the relative merits for selecting a single mechanism.

With the benefit of a computer design interface, a user can quickly scan the space of possible solutions, observe the mechanism motion and make a decision based on constraints such as the desired object trajectory or workspace obstructions. If the interface also provides information on the joint force index and driving forces for static and dynamic conditions, the designer has additional information for selecting a mechanism.

It is common for the kinematic synthesis process to produce a four-bar which has a desired motion of the object but is not well suited for driving with a motor at one of the fixed joints. For example, the mechanism may pass through a branch point or a joint

*Address all correspondence to this author.

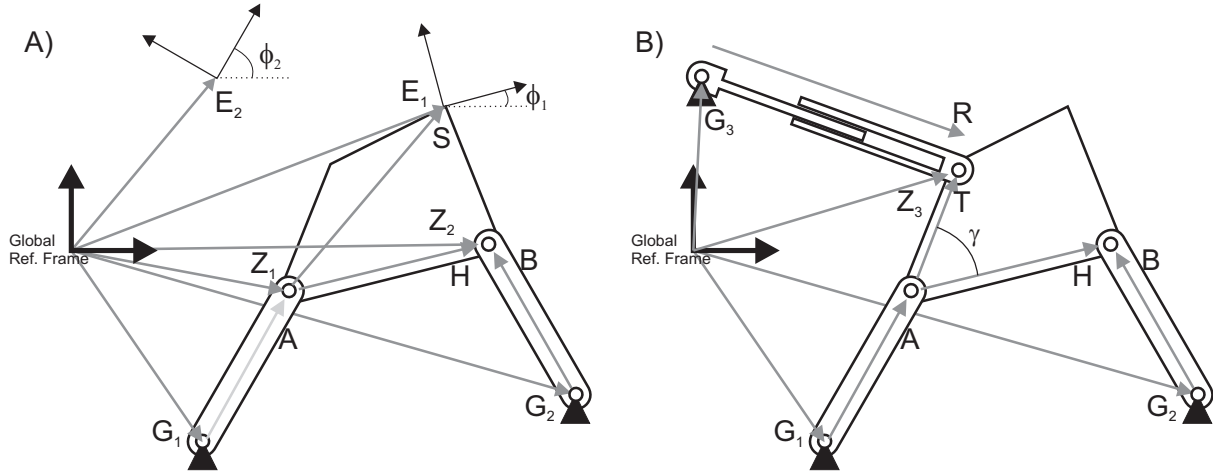


Figure 1. THE MECHANISM CAN BE DRIVEN TO THE TWO POSITIONS BY A TORQUE AT G_1 OR BY A FORCE ON THE PRISMATIC LINK

singularity as it moves from one configuration to the other. [4] One method of addressing this issue to add a driving dyad to the coupler, thereby separating the design of the motion profile with the four-bar from the force transmission design. In this paper, we look at adding an RPR leg between the ground link and the coupler producing a coupler driven four-bar, a modified version of the classic Stephenson III. Actuating the prismatic joint makes practical implementation more feasible, since the actuator could be a pneumatic, hydraulic or ball-screw linear actuator.

This work is part of a larger project to design and implement spherical four-bar mechanisms for two spatial orientation tasks. [5] [6] The spatial problem is less well studied and harder to intuitively visualize. The creation of the software for the planar case allowed us explore features of a good design interface and to examine the utility of some ideas, such as driving the four-bar with a prismatic chain, in the plane before extrapolating to the spherical case.

TWO POSITION SYNTHESIS

The two positions are defined with respect to a fixed reference frame as shown in Fig. 1-A. The vector \vec{E}_1 defines the x,y displacement of the the first position from the global reference frame and ϕ_1 defines the orientation with respect to the global x-axis. Similarly, \vec{E}_2 and ϕ_2 define the displacement and orientation for the second position.

A four-bar with a point on the coupler at \vec{E}_1 is defined in the first position by the two vector loop equations.

$$\vec{G}_1 + \vec{A} + \vec{H} = \vec{G}_2 + \vec{B} \quad (1)$$

$$\vec{G}_1 + \vec{A} + \vec{S} = \vec{E}_1 \quad (2)$$

In the second configuration, the four-bar is defined by the vector loop equation where the vectors \vec{H} and \vec{S} have been rotated by $\phi_2 - \phi_1$, and the vectors \vec{A} and \vec{B} are rotated by Δ_A and Δ_B respectively

$$\vec{G}_1 + Rot(\Delta_A)\vec{A} + Rot(\phi_2 - \phi_1)\vec{H} = \vec{G}_2 + Rot(\Delta_B)\vec{B} \quad (3)$$

$$\vec{G}_1 + Rot(\Delta_A)\vec{A} + Rot(\phi_2 - \phi_1)\vec{S} = \vec{E}_2 \quad (4)$$

$$\text{where } Rot(\theta) = \begin{bmatrix} \cos \theta & -\sin \theta \\ \sin \theta & \cos \theta \end{bmatrix}$$

The problem statement has fourteen values to define the mechanism (two each for the vectors \vec{G}_1 , \vec{G}_2 , \vec{A} , \vec{B} , \vec{H} and \vec{S} , plus the rotation angles Δ_A and Δ_B) with eight constraints from the vector equations 1-4. This leaves the designer with six values which can be freely chosen and the remaining eight derived to solve the problem. Searching the six-fold space of solutions to find a single preferred solution can be an arduous task without the assistance of a computer design interface or optimization.

DESIGN INTERFACE

The Planinator design interface¹ was written in MatlabTM and a screen shot is shown in Fig. 2. The top six slider bars are used to specify the two locations and orientations. These positions are displayed by showing the local x and y axes for the object reference frame. The next six slider bars are the design variables which the user is allowed to specify. We felt that the most natural input values would be the x and y location of each

¹The software can be downloaded from <http://www.engr.udayton.edu/faculty/amurray/PODS>

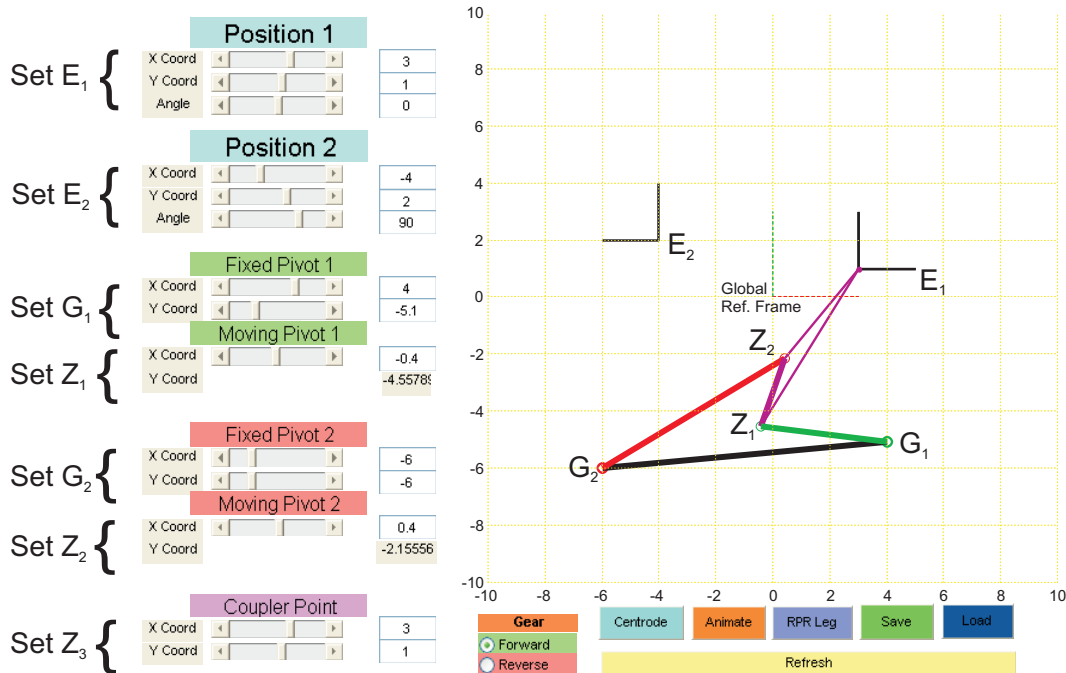


Figure 2. THE PLANINATOR INTERFACE ALLOWS THE USER TO DEFINE THE PROBLEM AND SEARCH THE SOLUTION SPACE

fixed pivot and the x location of each moving pivot in the first configuration. These choices gives the designer equal control over the left and right chains of the four-bar.

As the input values are changed, the program updates the values of the remaining variables based on the loop equations 1-4 and redraws the mechanism. The program also checks whether the two positions are on distinct circuits by checking the classification of the mechanism and the relative orientation of the vectors in the initial and final configurations according to Eqn. (5), and warns the designer if it fails by drawing the linkage entirely in red.

No defect if:

- Non-Grashof.
- Crank-Rocker AND

$$\text{sign}(\vec{B} \times \vec{H}) = \text{sign}(\text{Rot}(\Delta_B)\vec{B} \times \text{Rot}(\phi_2 - \phi_1)\vec{H})$$
- Rocker-Crank AND

$$\text{sign}(\vec{A} \times \vec{H}) = \text{sign}(\text{Rot}(\Delta_A)\vec{A} \times \text{Rot}(\phi_2 - \phi_1)\vec{H})$$
- Grashof Double-Rocker AND

$$\text{sign}(\vec{B} \times \vec{G}) = \text{sign}(\text{Rot}(\Delta_B)\vec{B} \times \vec{G})$$
- Triple-Crank AND

$$\text{sign}(\vec{B} \times \vec{H}) = \text{sign}(\text{Rot}(\Delta_B)\vec{B} \times \text{Rot}(\phi_2 - \phi_1)\vec{H})$$

(5)

The motion of the linkage can be observed by pressing the *Animate* button on the bottom of the window. If the *Forward* option is selected, the animation begins with joint at G_1 rotating counter-clockwise. The motion continues until the moving reference frame reaches the desired location or a joint limit for G_1 is reached. At the joint limit, the motion of the joint is reversed with the four-bar in the opposite branch configuration. If it reaches the other joint limit, it reverses again and reverts to the original branch configuration. In this way, the mechanism cycles through all reachable configurations. When the moving reference frame reaches the desired location, the animation stops. The *Reverse* option is identical except that the G_1 joint begins by rotating clockwise. Very often, one direction is notably shorter than the other. Fig. 3 shows the forward and reverse paths for the coupler point for one problem.

The designer can save and restore a particular solution by using the *Save* and *Load* buttons. Pressing the *Centrode* button produces a display of the moving centrode for the mechanism in the first configuration.

COUPLER DRIVEN FOUR-BAR

While the four-bar generated by the method described above will reach the two specified locations, it may not be a good mechanism for practical implementation with a motor on one of the fixed joints. The linkage may pass through a singularity where

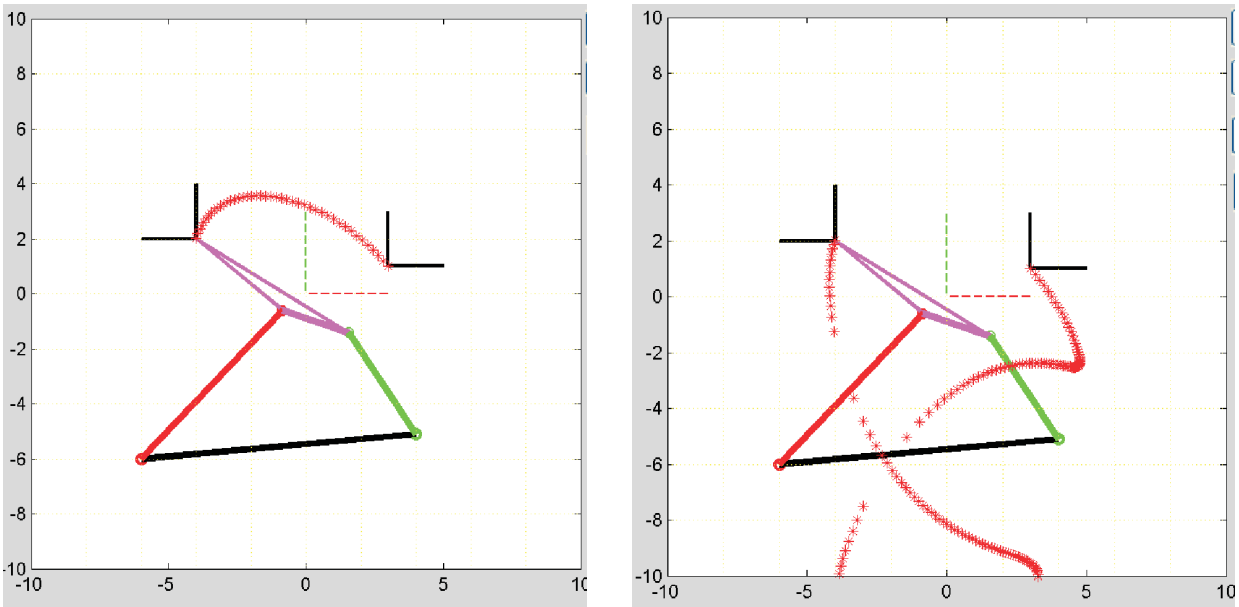


Figure 3. ONE DIRECTION TO DRIVE THE MECHANISM IS OFTEN MUCH SHORTER THAN THE OTHER

the motor would be unable to oppose a load applied to the coupler. If the two locations lie on different branches of the mechanism motion, the driving motor would need to move to the joint limit and then reverse direction along the opposite branch.

Based on this issue, we decided to explore the idea of using an RPR chain attached to the coupler to drive the motion. As shown in Fig. 1-B, the chain attaches to the ground link with a rotation joint at G_3 and to the coupler with a rotational joint at Z_3 . The length between G_3 and Z_3 can be changed with the prismatic joint between the two rotational joints. This is kinematically similar to the Stephenson III linkage, where an RRR dyad is attached to the coupler. [7] [8]

In the design software, the user can select the location of Z_3 using the final two slider bars on the interface. While Z_3 may be arbitrarily located on the coupler, it is often beneficial, for force balancing reasons, to choose a point near or on the load point E . After Z_3 has been selected, it is necessary to find a valid location for G_3 .

In order for the RPR chain to be able to drive the mechanism, the line of force from Z_3 to G_3 must not pass through the instant center of the coupler's motion. When the designer presses the RPR button on the interface, the program displays the window shown in Fig. 4-A. The program steps through the configurations of the mechanism as it moves from point 1 to point 2 and draws a red line defined by the instant center and Z_3 at each step. These red lines sweep out a region where it is unacceptable to place G_3 . It is possible for a given mechanism and Z_3 choice for no valid locations for G_3 to exist, particularly if the path of Z_3 or the

centrode are convoluted.

The designer can then select a location for G_3 in the window; at which point the graphic in Fig. 4-B is displayed. This shows the length of the RPR chain in each configuration. The salient information from this graph is that for a location of G_3 outside the swept red lines in Fig. 4-A, the prismatic joint is always monotonically increasing or monotonically decreasing, meaning that a linear actuator can be connected that will only increase to move the mechanism from point 1 to point 2 and only decrease to reverse (or vice versa).

JOINT FORCE INDEX

One common method for evaluating the quality of a particular linkage design is the *joint force index* or *JFI*. [9] [10] This is a measure of the largest load on any individual joint in the mechanism. It is a useful metric because the maximum force carried by a joint determines the type (and cost) of connection which can be used. A large JFI also indicates a poor force transmission configuration, since more of the input force from the actuator results in internal loading than in producing an external force at the coupler point.

The JFI metric was implemented in the design software to compare the coupler driven four-bar to the standard four-bar. After the design has selected a possible location for Z_3 and G_3 , the software calculates the JFI at each configuration of the mechanism for each of the three input methods (a torque at G_1 , a torque at G_2 or a force along the RPR chain).

Fig. 5-A shows the free body diagram of the four-bar mech-

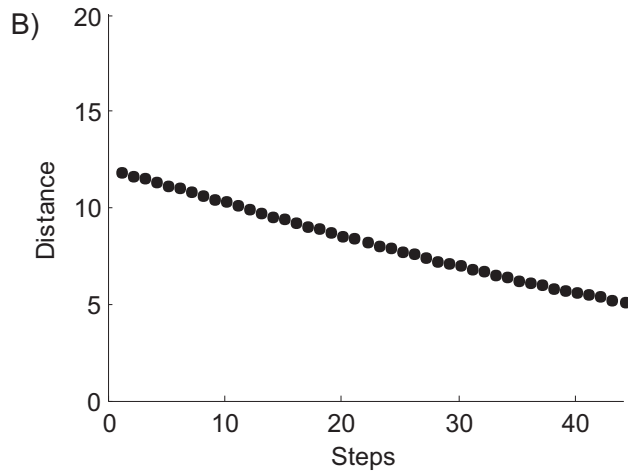
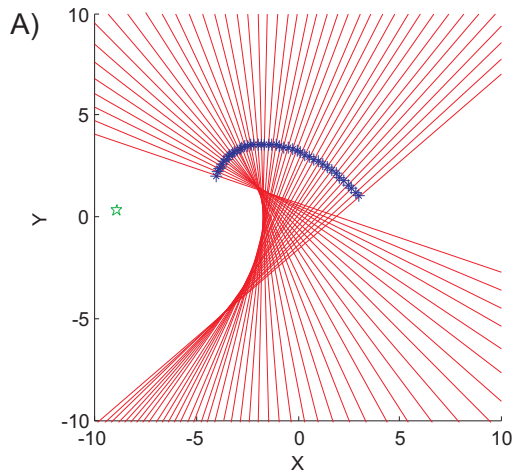


Figure 4. PLACING THE JOINT G_3 OUTSIDE THE RED ZONE RESULTS IN A MONOTONICALLY DRIVEN PRISMATIC JOINT

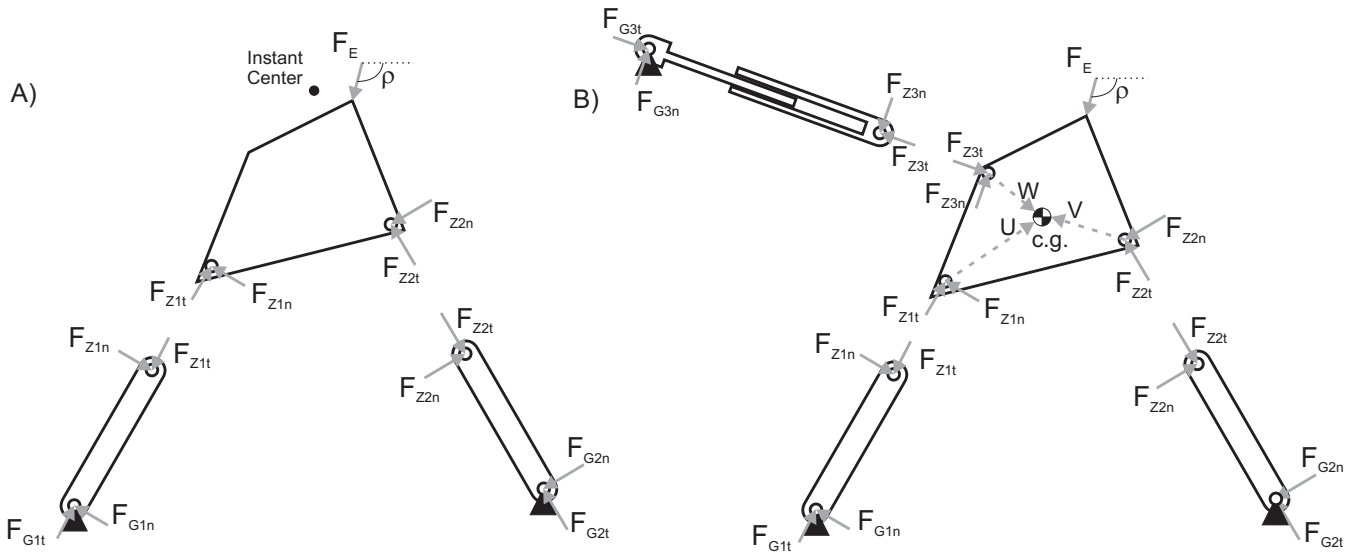


Figure 5. THE FREE-BODY DIAGRAMS FOR THE 4R AND THE COUPLER DRIVEN FOUR-BAR

anism. When the static balance is maintained by a torque at G_1 , the $F_{Z_{2n}}$ force is zero and $F_{Z_{1n}} = \tau a$ where τ is the input torque. The external load F_E is assumed to be applied at the point E in a direction tangential to the path of E . Loads normal to the path of E will only produce internal forces and are not a valid point of comparison. With the directions of the forces known, the magnitudes can be solved using the standard force balance equations on the coupler.

$$F_E \cos \rho + F_{Z_{1t}} \cos \theta_A + F_{Z_{2t}} \cos \theta_B - F_{Z_{1n}} \sin \theta_A = 0 \quad (6)$$

$$F_E \sin \rho + F_{Z_{1t}} \sin \theta_A + F_{Z_{2t}} \sin \theta_B + F_{Z_{1n}} \cos \theta_A = 0 \quad (7)$$

$$\vec{F}_E \times (\vec{E} - \vec{I}) + F_{Z_{1n}} \times (\vec{Z}_1 - \vec{I}) = 0 \quad (8)$$

$$\text{where } \begin{bmatrix} \cos \rho \\ \sin \rho \end{bmatrix} \times \frac{d\vec{E}}{dt} = 0$$

\vec{I} is the location of the coupler's instant center with respect to ground. The joint force on Z_2 is equal to $F_{Z_{2t}}$, and the joint force on Z_1 is $\sqrt{(F_{Z_{1n}})^2 + (F_{Z_{1t}})^2}$. A similar process is followed to find the joint forces if the mechanism is driven by a torque on G_2 .

Fig. 5-B shows the free body diagram for the coupler when driven by a force along the RPR chain. As above, the external load is applied at E and is tangential to the path of E . Under static conditions, $F_{Z_{1n}} = F_{Z_{1t}} = F_{Z_{2n}} = 0$. The coupler static load

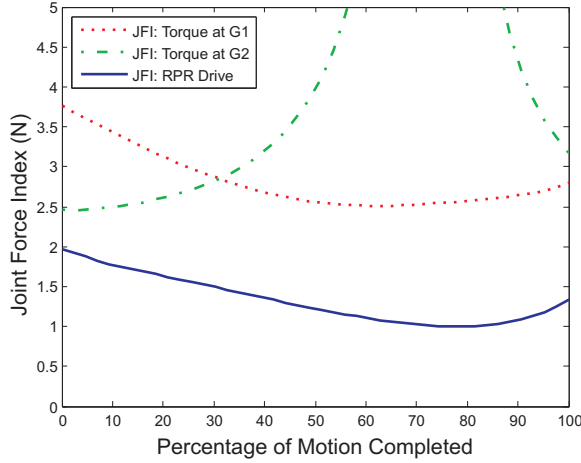


Figure 6. A WELL CHOSEN RPR LEG USUALLY PRODUCES A LOWER JFI THAN A TORQUE DRIVE

balance equations are:

$$F_E \cos \rho + F_{Z_{1t}} \cos \theta_A + F_{Z_{2t}} \cos \theta_B + F_{Z_{3t}} \sin \theta_R = 0 \quad (9)$$

$$F_E \sin \rho + F_{Z_{1t}} \sin \theta_A + F_{Z_{2t}} \sin \theta_B + F_{Z_{3t}} \cos \theta_R = 0 \quad (10)$$

$$\vec{F}_E \times (\vec{E} - \vec{I}) + F_{Z_{3t}} \times (\vec{Z}_3 - \vec{I}) = 0 \quad (11)$$

The design software calculates the joint forces throughout the motion for a nominal external load of 1 N for each input setup and graphs the results. An example output is shown in Fig. 6.

SYSTEM DYNAMICS OF COUPLER DRIVEN FOUR-BAR

To properly evaluate the operational requirements of the mechanism, it is necessary to look at the dynamic properties of the system. Since the dynamics of a four-bar are well examined, we will focus on the derivation of the dynamics for the coupler driven four-bar. The process begins with the loop closure equations as defined by Fig. 1 shown in Eqns. (12)-(15).

The position loop values are known throughout the range of motion from the synthesis procedure above. Taking the derivative of the position loop generates Eqn. (16), the velocity loop for the mechanism written in matrix form to separate the passive joint velocities from the input velocity \dot{r} , the rate of change in length of link R .

For a given input joint velocity in a given configuration, the passive joint velocities can be found by inverting the matrix in Eqn. (16). Once the velocities are known, the second derivative of the position loop can be set up to find the passive joint accel-

erations in terms of the input acceleration \ddot{r} . These equations are shown in matrix form in Eqn. (18).

Inverting the matrix in Eqn. (18) produces linear equations for the angular accelerations of the form

$$\alpha_A = K_1 \ddot{r} + K_2 \quad (27)$$

$$\alpha_H = K_3 \ddot{r} + K_4 \quad (28)$$

$$\alpha_B = K_5 \ddot{r} + K_6 \quad (29)$$

$$\alpha_R = K_7 \ddot{r} + K_8 \quad (30)$$

where the values of the coefficients K_i are known for a given position and velocity of the mechanism.

The dynamic force equations for each link, based on the free body diagrams in Fig. 5 are shown in Eqns. (19)-(26).

Using the substitutions for the angular accelerations in terms of \ddot{r} from Eqns. (27)-(30), the dynamic equations become twelve equations with twelve unknown forces and the unknown acceleration \ddot{r} . If either the input force $F_{Z_{3t}}$ or the desired acceleration is specified, the remaining forces can be calculated. It should be noted that Eqns. (19)-(26) assume the centers of mass for links A, B and R lie at the midpoint of the links.

In the design interface, when the user has selected Z_3 and G_3 locations for the RPR chain, she has the option of examining the dynamics of the mechanism. The program calculates the required force to drive the mechanism from point 1 to point 2 in two seconds. To eliminate force spikes, the velocity, acceleration and jerk of the prismatic joint are all zero at the start and end of motion by requiring the length of link R to be a sigmoid function of time.

When the program has completed the calculations, it displays to the designer the maximum force of the prismatic joint, the maximum power output by the prismatic joint and the maximum joint force index over the range of motion. This information allows the designer to compare the performance of two different mechanisms in an operation where dynamic forces dominate. (Some assumptions about the mass and moments of inertia of each link were necessary, but since the assumptions were based on the size of the links and consistent for all mechanisms, the comparisons should be valid.)

EVALUATION AND CONCLUSION

The design software successfully allowed the designer to navigate the space of solutions to the two position problem. It also provided means to allow the designer to compare solutions to the problem based on the kinematics, the statics and the dynamics.

Some improvements to the interface could be made. The design input variables on the slider bars made it possible to skim

Position Loop

$$g_1 \cos \theta_{G_1} + a \cos \theta_A + h \cos \theta_H - b \cos \theta_B - g_2 \cos \theta_{G_2} = 0 \quad (12)$$

$$g_1 \sin \theta_{G_1} + a \sin \theta_A + h \sin \theta_H - b \sin \theta_B - g_2 \sin \theta_{G_2} = 0 \quad (13)$$

$$g_1 \cos \theta_{G_1} + a \cos \theta_A + t \cos(\theta_H + \gamma) - r \cos \theta_R - g_3 \cos \theta_{G_3} = 0 \quad (14)$$

$$g_1 \sin \theta_{G_1} + a \sin \theta_A + t \sin(\theta_H + \gamma) - r \sin \theta_R - g_3 \sin \theta_{G_3} = 0 \quad (15)$$

Velocity Loop

$$\begin{bmatrix} -a \sin \theta_A & -h \sin \theta_H & b \sin \theta_B & 0 \\ a \cos \theta_A & h \cos \theta_H & -b \cos \theta_B & 0 \\ -a \sin \theta_A & -t \sin(\theta_H + \gamma) & 0 & r \sin \theta_R \\ a \cos \theta_A & t \cos(\theta_H + \gamma) & 0 & -r \cos \theta_R \end{bmatrix} \begin{bmatrix} \omega_A \\ \omega_H \\ \omega_B \\ \omega_R \end{bmatrix} = \begin{bmatrix} 0 \\ 0 \\ \dot{r} \cos \theta_R \\ \dot{r} \sin \theta_R \end{bmatrix} \quad (16)$$

Acceleration Loop

$$\begin{bmatrix} -a \sin \theta_A & -h \sin \theta_H & b \sin \theta_B & 0 \\ a \cos \theta_A & h \cos \theta_H & -b \cos \theta_B & 0 \\ -a \sin \theta_A & -t \sin(\theta_H + \gamma) & 0 & r \sin \theta_R \\ a \cos \theta_A & t \cos(\theta_H + \gamma) & 0 & -r \cos \theta_R \end{bmatrix} \begin{bmatrix} \alpha_A \\ \alpha_H \\ \alpha_B \\ \alpha_R \end{bmatrix} = \begin{bmatrix} a\omega_A^2 \cos \theta_A + h\omega_H^2 \cos \theta_H - b\omega_B^2 \cos \theta_B \\ a\omega_A^2 \sin \theta_A + h\omega_H^2 \sin \theta_H - b\omega_B^2 \sin \theta_B \\ a\omega_A^2 \cos \theta_A + t\omega_H^2 \cos(\theta_H + \gamma) - r\omega_R^2 \cos \theta_R - 2\dot{r}\omega_R \sin \theta_R + \ddot{r} \cos \theta_R \\ a\omega_A^2 \sin \theta_A + t\omega_H^2 \sin(\theta_H + \gamma) - r\omega_R^2 \sin \theta_R + 2\dot{r}\omega_R \cos \theta_R + \ddot{r} \sin \theta_R \end{bmatrix} \quad (17)$$

Force Balance Equations

$$\vec{F}_{Z_{1n}} + \vec{F}_{Z_{1t}} + \vec{F}_{G_{1n}} + \vec{F}_{G_{1t}} = m_A \frac{a}{2} \left(\omega_A^2 \begin{bmatrix} -\cos \theta_A \\ -\sin \theta_A \end{bmatrix} + \alpha_A \begin{bmatrix} -\sin \theta_A \\ \cos \theta_A \end{bmatrix} \right) \quad (19)$$

$$\frac{1}{2} \left(\vec{F}_{Z_{1n}} \times \vec{A} + \vec{F}_{G_{1n}} \times \vec{A} \right) = I_A \alpha_A \quad (20)$$

$$\vec{F}_{Z_{2n}} + \vec{F}_{Z_{2t}} + \vec{F}_{G_{2n}} + \vec{F}_{G_{2t}} = m_B \frac{b}{2} \left(\omega_B^2 \begin{bmatrix} -\cos \theta_B \\ -\sin \theta_B \end{bmatrix} + \alpha_B \begin{bmatrix} -\sin \theta_B \\ \cos \theta_B \end{bmatrix} \right) \quad (21)$$

$$\frac{1}{2} \left(\vec{F}_{Z_{2n}} \times \vec{B} + \vec{F}_{G_{2n}} \times \vec{B} \right) = I_B \alpha_B \quad (22)$$

$$\vec{F}_{Z_{3n}} + \vec{F}_{Z_{3t}} + \vec{F}_{G_{3n}} + \vec{F}_{G_{3t}} = m_R \frac{r}{2} \left(\omega_R^2 \begin{bmatrix} -\cos \theta_R \\ -\sin \theta_R \end{bmatrix} + \alpha_R \begin{bmatrix} -\sin \theta_R \\ \cos \theta_R \end{bmatrix} \right) \quad (23)$$

$$\frac{1}{2} \left(\vec{F}_{Z_{3n}} \times \vec{R} + \vec{F}_{G_{3n}} \times \vec{R} \right) = I_R \alpha_R \quad (24)$$

$$\vec{F}_{Z_{1n}} + \vec{F}_{Z_{1t}} + \vec{F}_{Z_{2n}} + \vec{F}_{Z_{2t}} + \vec{F}_{Z_{3n}} + \vec{F}_{Z_{3t}} = m_C \left(a\alpha_A \begin{bmatrix} -\sin \theta_A \\ \cos \theta_A \end{bmatrix} + a\omega_A^2 \begin{bmatrix} -\cos \theta_A \\ -\sin \theta_A \end{bmatrix} + u\alpha_U \begin{bmatrix} -\sin \theta_U \\ \cos \theta_U \end{bmatrix} + u\omega_U^2 \begin{bmatrix} -\cos \theta_U \\ -\sin \theta_U \end{bmatrix} \right) \quad (25)$$

$$\left(\vec{F}_{Z_{1n}} + \vec{F}_{Z_{1t}} \right) \times \vec{U} + \left(\vec{F}_{Z_{2n}} + \vec{F}_{Z_{2t}} \right) \times \vec{V} + \left(\vec{F}_{Z_{3n}} + \vec{F}_{Z_{3t}} \right) \times \vec{W} = I_C \alpha_C \quad (26)$$

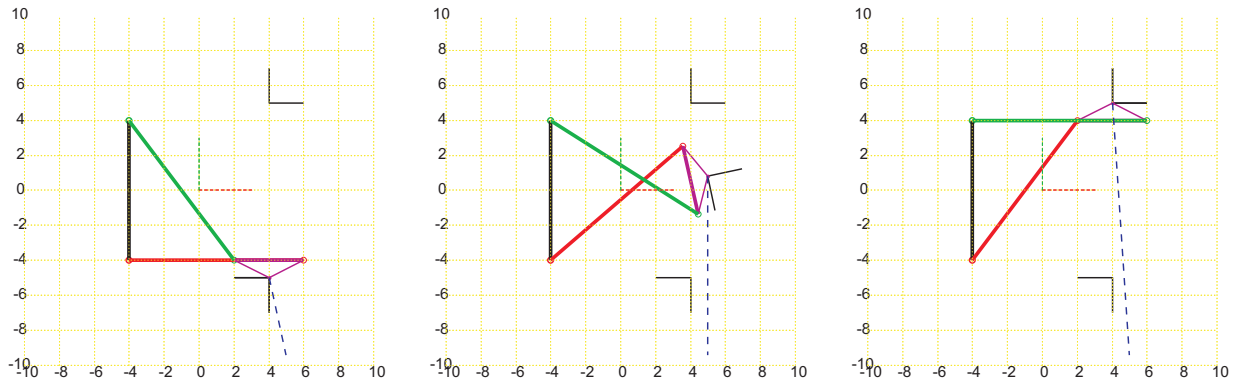


Figure 7. DRIVING A LINKAGE WITH AN RPR LEG OFTEN IMPROVES PERFORMANCE

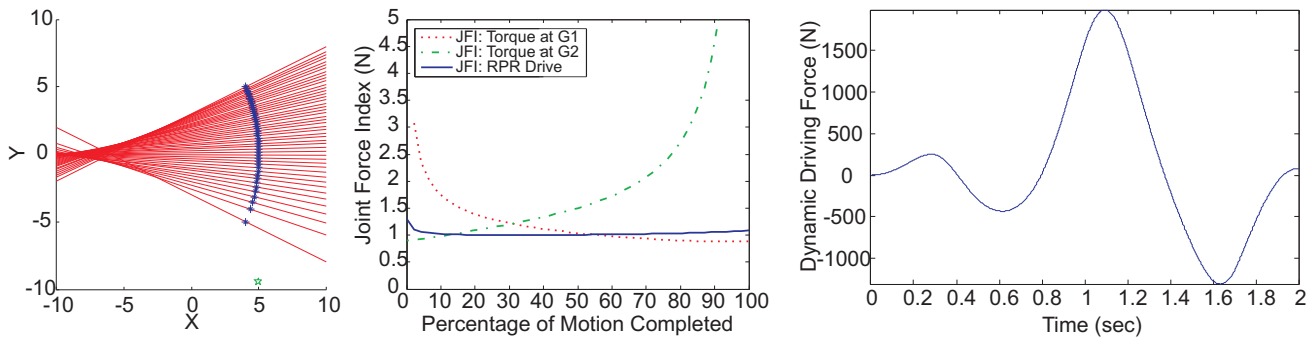


Figure 8. THE SOFTWARE PROVIDES THE DESIGNER WITH USEFUL INFORMATION TO EVALUATE A MECHANISM

through multiple designs, but did make it hard to find a design to match a pre-conceived idea. The selection of locations for Z_3 and G_3 could be frustrating, since the software regenerated the plot of valid G_3 locations every time before showing the joint-force index or dynamic force information. Some of these improvements are being implemented in the next generation of software for working with the spatial problem.

The software did improve the researcher's understanding of the value of the coupler driven four-bar idea. In general, there is an RPR chain which results in a lower joint force index than for the four-bar driven by a torque at the fixed joint, largely due to dividing the load forces over three joints instead of two. The RPR chain works best when Z_3 is placed at or near the load point E , and when the path of E is "smooth". If the two positions are on different branches of the four-bar motion for the input torque, then a well placed RPR is significantly better.

Figure 7 shows an example where the RPR chain avoids branching issues. For the task shown, where the two positions include a 180° rotation, the selected four-bar solves the problem

with a smooth trajectory. It would be difficult to drive the linkage with a torque at either fixed pivot, since each position is a branch point for one of the rotating links. We added an RPR chain with the moving pivot at the moving reference frame and the fixed pivot selected at the star in Fig. 8-A to be in line with the motion of the coupler. This creates a much lower joint force index, as shown in 8-B. The dynamic force load in Fig. 8-C shows a peak force in the prismatic joint of 2000 N for comparison to other mechanisms. This value is lower than for other nearby choices for G_3 because the driving force is tangent to the coupler path at the point of greatest acceleration and velocity.

These and other insights have demonstrated to the researcher the value of being able to explore and evaluate the solution space quickly. These ideas are currently being evaluated for the spatial mechanism application.

ACKNOWLEDGMENT

This material is based upon work supported by the National Science Found-

dition under Grants No. #0422731. The authors also extend their gratitude to Thomas Kennicott and Robert Douglas for their insights into automated assembly practices

REFERENCES

- [1] Norton, R., 2001. *Design of Machinery*. McGraw-Hill, New York, NY.
- [2] Waldron, K., and Kinzel, G., 1999. *Kinematics, Dynamics and Design of Machinery*. John Wiley & Sons, New York, NY.
- [3] McCarthy, M. J., 2000. *Geometric Design of Linkages*. Springer-Verlag, New York, NY.
- [4] Chase, T., and Mirth, J., 1993. "Circuits and branches of single degree-of-freedom planar linkages". *ASME Journal of Mechanical Design*, **115**(2), pp. 222–230.
- [5] Perry, L., Turner, M., and Murray, A., 2002. "The kinematic synthesis of a two spatial position, two velocity problem involving a spherical mechanism". *Proceedings of the 2002 ASME Design and Technical Conference*.
- [6] Turner, M. L., Perkins, D., Murray, A., and Larochelle, P., 2005. "Systematic process for constructing four-bar spherical mechanisms". *Proceedings of the 2005 ASME IMECE Conference*, November.
- [7] Watanabe, K., and Funabashi, H., 1984. "Kinematic analysis of stephenson six-link mechanisms - discrimination of composition loops". *Bulletin of JSME*, **27**(234), December, pp. 2863–2870.
- [8] Mirth, J., and Chase, T., 1992. "Circuit rectification for four precision position synthesis of stephenson six-bar linkages". *ASME Journal of Mechanical Design*, **117**(4), pp. 644–645.
- [9] Watanabe, K., and Funabashi, H., 1984. "Kinematic analysis of stephenson six-link mechanisms - transmission characteristics". *Bulletin of JSME*, **27**(234), December, pp. 2871–2879.
- [10] Lin, C., and Chang, W., 2002. "The force transmissivity index of planar linkage mechanisms". *Mechanism and Machine Theory*, **37**, pp. 1465–1485.